PORTLAND PRESS

Research Article

PINK1-dependent phosphorylation of Serine111 within the SF3 motif of Rab GTPases impairs effector interactions and LRRK2-mediated phosphorylation at Threonine72

Sophie Vieweg[1],*, Katie Mulholland[2],*, Bastian Bräuning[1], Nitin Kachariya[1], Yu-Chiang Lai[2], Rachel Toth[2], Pawan Kishor Singh[2], Ilaria Volpi[2], Michael Sattler[1,3], Michael Groll[1], Aymelt Itzen[1,4] and ⓘ Miratul M. K. Muqit[2]

[1]Department of Chemistry, Centre for Integrated Protein Science Munich (CIPSM), Technical University of Munich, Garching 85748, Germany; [2]MRC Protein Phosphorylation and Ubiquitylation Unit, School of Life Sciences, University of Dundee, Dundee, U.K.; [3]Institute of Structural Biology, Helmholtz Zentrum München, 85764 Neuherberg, Germany; [4]Center for Experimental Medicine, Institute of Biochemistry and Signal Transduction, Universitätsklinikum Hamburg-Eppendorf (UKE), Hamburg 20246, Germany

Correspondence: Michael Groll (michael.groll@ch.tum.de), Aymelt Itzen (a.itzen@uke.de) or Miratul M. K. Muqit (m.muqit@dundee.ac.uk)

OPEN ACCESS

Loss of function mutations in the PTEN-induced kinase 1 (PINK1) kinase are causal for autosomal recessive Parkinson's disease (PD) whilst gain of function mutations in the LRRK2 kinase cause autosomal dominant PD. PINK1 indirectly regulates the phosphorylation of a subset of Rab GTPases at a conserved Serine111 (Ser111) residue within the SF3 motif. Using genetic code expansion technologies, we have produced stoichiometric Ser111-phosphorylated Rab8A revealing impaired interactions with its cognate guanine nucleotide exchange factor and GTPase activating protein. In a screen for Rab8A kinases we identify TAK1 and MST3 kinases that can efficiently phosphorylate the Switch II residue Threonine72 (Thr72) in a similar manner as LRRK2 in vitro. Strikingly, we demonstrate that Ser111 phosphorylation negatively regulates the ability of LRRK2 but not MST3 or TAK1 to phosphorylate Thr72 of recombinant nucleotide-bound Rab8A in vitro and demonstrate an interplay of PINK1- and LRRK2-mediated phosphorylation of Rab8A in transfected HEK293 cells. Finally, we present the crystal structure of Ser111-phosphorylated Rab8A and nuclear magnetic resonance structure of Ser111-phosphorylated Rab1B. The structures reveal that the phosphorylated SF3 motif does not induce any major changes, but may interfere with effector-Switch II interactions through intramolecular H-bond formation and/or charge effects with Arg79. Overall, we demonstrate antagonistic regulation between PINK1-dependent Ser111 phosphorylation and LRRK2-mediated Thr72 phosphorylation of Rab8A indicating a potential cross-talk between PINK1-regulated mitochondrial homeostasis and LRRK2 signalling that requires further investigation in vivo.

Introduction

Autosomal recessive mutations in PTEN-induced kinase 1 (PINK1) represent the second most frequent cause of early onset Parkinson's disease (PD) [1]. PINK1 encodes a protein kinase that is localized to the mitochondria via an N-terminal mitochondrial targeting domain. In response to chemical uncouplers (e.g. carbonyl cyanide m-chlorophenyl hydrazone (CCCP)) that induce mitochondrial depolarization, PINK1 is activated and directly phosphorylates Parkin at Serine 65 (Ser65) within its N-terminal Ubiquitin-like domain [2,3] as well as the equivalent Ser65 residue of ubiquitin [4–7]. The

phosphorylation of both of these residues is required for maximal activation of Parkin E3 ligase activity that induces ubiquitylation of a myriad of substrates and acts as a signal for the elimination of damaged mitochondria via mitophagy [4–7].

Previous work has shown that upon activation, PINK1 indirectly induces the phosphorylation of a subset of Rab GTPases including Rab 1B, 8A, 8B and 13 at a highly conserved Serine residue (Ser111 in Rab8A) that lies within the RabSF3 motif [8]. Of relevance to PD mechanisms, loss of function mutations of PINK1 abolish Rab protein phosphorylation as assessed in primary mouse embryonic fibroblasts from PINK1 knockout mice or human adult fibroblasts derived from patients harbouring homozygous PINK1 Q456X mutations [8].

Recent studies have also linked other Parkinson's genes to the regulation of Rab proteins. Autosomal dominant activating mutations of LRRK2 represent the most frequent genetic cause of familial PD accounting for ~5% of all cases and clinical LRRK2 inhibitor trials have recently started (Denali Therapeutics). LRRK2 phosphorylates a highly conserved threonine residue within the Switch II domain of 14 Rab GTPase isoforms (Thr72 in Rab8A) that lies upstream of the PINK1-regulated Ser111 site [9,10]. Furthermore, autosomal dominant missense mutations of the vacuolar protein sorting-associated protein VPS35 (D620N) are associated with a substantial elevation of LRRK2-mediated Rab phosphorylation [11].

The identity of the upstream Rab Ser111 kinase remains unknown and this has hampered progress to determine the impact of PINK1-dependent Ser111 phosphorylation on the function of Rab GTPases. Another open question is whether PINK1 lies in signalling networks with other PD gene pathways. Herein we undertake a screen to identify Rab protein kinases and discover that TAK1 and MST3 can efficiently phosphorylate Thr72 equivalent to the LRRK2 site *in vitro*. Furthermore, we have employed genetic code expansion technologies to produce milligram quantities of Ser111-phosphorylated Rab8A and Rab1B that has enabled our investigation of how phosphorylation affects Rab function, and has revealed an antagonistic role between PINK1 and LRRK2-mediated phosphorylation of Rabs.

Materials and methods

Reagents

$[\gamma\text{-}^{32}P]$ ATP was from PerkinElmer, MLi-2 was obtained from Merck [12]. LRRK2 (G2019S) Recombinant Human Protein (residues 970–2527 #10499963) was purchased from Invitrogen and all additional kinases used in the *in vitro* screen were from MRC PPU Reagents and Services — including TAK1 (1–303), TAB1 (437–504) fusion (DU753) and N-terminal GST-MST3 (DU30889). All mutagenesis was carried out using the QuikChange site-directed mutagenesis method (Stratagene) with KOD polymerase (Novagen). All DNA constructs were verified by DNA sequencing, which was performed by The Sequencing Service, School of Life Sciences, University of Dundee, using DYEnamic ET terminator chemistry (Amersham Biosciences) on Applied Biosystems automated DNA sequencers. DNA for bacterial protein expression was transformed into *E. coli* BL21 DE3 RIL (codon plus) cells (Stratagene). All cDNA plasmids, antibodies and recombinant proteins generated for this study are available to request through our reagents website https://mrcppureagents.dundee.ac.uk/ or from the Itzen laboratory.

Expression of non-phosphorylated (WT) Rab proteins

WT-Rab1B (3–174) was expressed in fusion with a N-terminal His_6-MBP tag (pMAL) or a C-terminal His_6 tag (pNHD), while WT-Rab8A (6–176) was fused to a N-terminal His_6 tag or a C-terminal His_6 tag (pET19). The N-terminal Rab1B and Rab8A fusion constructs contained a TEV cleavage site to remove the His_6-MBP tag or His_6 tag from the N-terminus of the Rab proteins. The C-terminal His_6 tags remained on the Rab proteins. All WT-Rab proteins were expressed in BL21(DE3) *E. coli* in LB medium at 25°C overnight, and their expression was induced with 0.5 mM IPTG at OD_{600nm} = 0.8. In contrast with the Rab1B proteins, the Rab8A proteins were co-expressed with the chaperone GroEL/S (pGro7, Takara). The expression of the GroEL/S chaperone was auto-induced by supplementing the LB-medium with 1 mg/ml arabinose.

Phosphorylation of Rab proteins by genetic code expansion

For the incorporation of phospho-serine (pSer) during the expression of Rab1B (3–174) and Rab8A (6–176) proteins, we have employed a genetic code expansion strategy published by Rogerson *et al.* [13]. For this purpose, we introduced an amber stop codon at the amino acid position Ser111 via site-specific mutagenesis. We co-transformed the obtained constructs, Rab1B(S111(TAG))-His_6 (pNHD) and Rab8A(S111(TAG))-His_6

(pNHD), together with the pKW2 plasmid encoding for the orthogonal tRNA/tRNA-synthetase pair (SepRS (2)/pSer tRNA(B4)CUA) and the optimized elongation factor EF-Sep into the ΔserB-BL21(DE3) *E. coli* expression strain. In the case of pSer111-Rab8A, a third plasmid encoding for the GroEL/S chaperone (pET19) was transformed into the expression strain. The cells were grown in TB medium at 37°C and 180 rpm. The culture was supplemented with 2 mM O-Phospho-L-serine (Sigma) at $OD_{600nm} = 0.3$. The expression of all plasmids was induced simultaneously by the addition of 1 mM IPTG at $OD_{600nm} = 0.8$–0.9. The expression was carried out overnight at 30°C for pSer111-Rab1B and at 25°C for pSer111-Rab8A.

Purification of Rab proteins

Cells were harvested and resuspended in buffer A (50 mM HEPES, 500 mM LiCl, 10 mM imidazole, 1 mM $MgCl_2$, 10 μM GDP, 2 mM β-mercaptoethanol, pH 8.0) containing 1 mM PMSF and DNaseI. Cells were lysed on ice by sonication (60% amplitude, 5 min, pulse 5 s on and 15 s off), and insoluble cell debris was removed by centrifugation (48 254.4×*g*, 45 min, 4°C). All Rab proteins were purified from the supernatant by nickel affinity chromatography (5 ml HiTrap™ Chelating HP column, GE Healthcare). Non-specifically bound proteins were removed by a step wash with buffer B (50 mM HEPES, 500 mM LiCl, 500 mM imidazole 1 mM $MgCl_2$, 10 μM GDP, 2 mM β-mercaptoethanol, pH 8.0): 5% buffer B to remove impurities from non-phosphorylated (WT) Rab proteins, or three consecutive washes with 3%, 5% and 7% buffer B to purify phosphorylated Rab proteins, respectively. WT-Rab proteins eluted with a linear gradient from 5% to 60% buffer B in 100 ml, and phosphorylated Rab proteins eluted with a linear gradient from 7% to 50% buffer B in 50 ml. The collected fractions were analyzed by SDS–PAGE. Fractions containing the desired His_6-tagged protein were concentrated to 2 ml using Amicon® Ultra Centrifugal Filters (10000 MWCO, Merck Millipore), and were directly injected into a size-exclusion chromatography column (Superdex 75 16/60, GE Healthcare) equilibrated with buffer C (20 mM HEPES, 50 mM NaCl, 1 mM $MgCl_2$, 10 μM GDP, 1 mM DTT, pH 7.5). The purity of the fractions from the size-exclusion chromatography was determined by SDS–PAGE, and the clean fractions were pooled, concentrated using Amicon® Ultra Centrifugal Filters (10000 MWCO, Merck Millipore), and frozen in liquid nitrogen. The protein identity and integrity was confirmed by LC–MS. Note that Rab proteins with a N-terminal His_6 tag or His_6-MBP tag were treated with TEV protease after the nickel affinity purification, and dialyzed against 5l of buffer D (20 mM HEPES, 100 mM NaCl, 10 μM GDP, 2 mM β-mercaptoethanol, pH 8.0) at 4°C overnight. The cleaved N-terminal tags were separated from the Rab proteins by a second nickel affinity purification prior to the size-exclusion chromatography.

Nucleotide exchange of Rab proteins

The active form of Rab proteins was prepared by incubating the Rab proteins with 5 mM EDTA and 20 molar equivalents of GppNHp or GTP at 25°C for 3 h. The excess nucleotide was removed by buffer exchange using NAP5 columns (GE healthcare) or size-exclusion chromatography columns (Superdex 75 10/300, GE Healthcare) equilibrated with buffer E (20 mM HEPES, 50 mM NaCl, 1 mM $MgCl_2$, 10 μM GTP or GppNHp, 1 mM DTT, pH 7.5). The nucleotide loading of the Rab proteins was determined by C18 RP-HPLC. Therefore, 50 μM of Rab protein were heat denatured at 95°C for 5 min and spun down at maximum speed. The supernatant was injected into a C18 column equilibrated with 50 mM KPi (pH 6.6), 10 mM tetra-n-butylammonium bromide and 17% ACN. A mixture of guanosine nucleotides (GMP, GDP and GTP) and pure GppNHp were used as standards to determine the nucleotide loading state of the Rab proteins.

Guanosine nucleotide exchange factor (GEF) and GTPase activating protein (GAP) activity assay

GDP- or GTP-bound Rab proteins were diluted in buffer F (20 mM HEPES, 50 mM NaCl, 1 mM $MgCl_2$, pH 7.5) to a concentration of 4 μM, and transferred into a Quartz SUPRASIL cuvette (Hellma Analytics, Germany). The intrinsic tryptophane (Trp) fluorescence was recorded at 348 nm (ex = 297 nm) at 25°C with a Fluoromax-4 fluorescence spectrometer (HORIBA Jobin Yvon). When the Trp fluorescence signal stabilized, 50 μM of GTP were added into the cuvette containing 4 μM of Rab:GDP followed by the addition of a GEF enzyme (0.04 μM DrrA or 2 μM Rabin8) to record the nucleotide exchange reaction (GDP → GTP). To monitor the GTP hydrolysis reaction, 0.04 μM of the GAP TBC1D20 were mixed into 4 μM Rab:GTP. Based on the decrease or increase in Trp fluorescence over time, the GDP–GTP exchange rates and GTP hydrolysis rates (k_{obs}) were calculated for each Rab protein using the following exponential equation:

$y = y_0 + A \cdot e^{-k(t-t_0)} y_0$, final fluorescence value (end point) A, amplitude of fluorescence change t, time in seconds t_0 and initial time point of the reaction.

Isothermal titration calorimetry (ITC)

Rab8A-Mical-1 binding studies were conducted with a MicroCal PEAQ-ITC device (Malvern Instruments Ltd, U.K.). WT-Rab8A-His$_6$ and pSer111-Rab8A-His$_6$ were loaded with GppNHp as described above, and afterwards dialyzed together with Mical-1 against 5l of buffer G (20 mM HEPES, 50 mM NaCl, 2 mM MgCl$_2$, 1 mM TCEP, pH 7.5) at 4°C overnight. To determine the dissociation constant (K_D), 400 μM of WT-Rab8A-His$_6$: GppNHp or pSer111-Rab8A-His$_6$:GppNHp were titrated into the cell containing 40 μM of Mical-1. We performed 26 injections of 1.5 μl with a spacing of 120 s at 500 rpm stirring speed at 25°C. The data analysis was carried out with the integrated MicorCal software, and the raw data were fitted to a one-site binding model. For every experiment one technical replicate was recorded.

Thermal shift assay (TSA)

The thermal stability or melting temperatures (T_m) of the Rab proteins was determined using a SYPRO® orange-based TSA. Therefore, 2 μg of Rab protein were mixed with 5× SYPRO® orange protein gel stain (Sigma) in a volume of 20 μl. The TSA assay was performed in a CFX Connect™ real-time system (Bio-Rad) using a stepwise temperature increase from 25°C to 95° in 1°C per min (71 cycles). The excitation wavelength was set to 470 nm and emission was detected at 570 nm. The raw data were plotted (fluorescence F vs. temperature T) in Excel, and the T_m values (inflection points) were derived from the second derivate ($f''(T) = 0$) of each data set.

Liquid chromatography mass spectrometry (LC–MS)

Protein samples (0.1 mg/ml, 1 μl) were injected with an UltiMate3000® HPLC system (UHPLC$^+$ focused, Dionex) into a ProSwift™ RP-4H column (1× 50 mm, Thermo) at a flow rate of 0.7 ml/min. The proteins eluted with a linear gradient of 5–100% acetonitrile (0.1% formic acid) in 6 min. The desalted samples were ionized and analyzed by a LCQ fleet™ system (Thermo) combining electro spray ionization with an ion trap mass analyzer.

Phos-tag™ acrylamide gel analysis

SDS–PAGE gels (12% acrylamide) were prepared with 50 μM Phos-tag™ Acrylamide AAL-107, a phosphate-binding compound from Wako, and 100 μM MnCl$_2$. Five hundred nanograms of the phosphorylated Rab1B proteins (GDP/GppNHp) were loaded on the gel, together with the non-phosphorylated Rab1B proteins as negative controls.

Kinase assays

LRRK2 kinase assays were based on previous assay [10]. Assays were performed with a final volume of 25 μl with 2 μg Rab8A substrate, 100 ng LRRK2 G2019S (PV4881 Fisher Scientific), in 50 mM Tris–HCl (pH 7.5), 10 mM MgCl$_2$ and 0.1 mM [γ-^{32}P] ATP (∼300–500 c.p.m./pmol, PerkinElmer) in the absence or presence of MLi-2 (1 μM). Assays were incubated for 30 min at 30°C, with shaking at 1050 r.p.m. and quenched through addition of SDS sample loading buffer with 1% beta-mercaptoethanol and heating at 75°C for 10 min. Reaction mixtures were resolved by SDS–PAGE. Proteins were detected by Coomassie staining and gels imaged with an Epson scanner, prior to gel drying (Bio-Rad). Incorporation of [γ-^{32}P] ATP into substrates was analyzed by autoradiography, using Amersham hyperfilm. Quantification of [γ-^{32}P] ATP into substrates was performed by Cerenkov counting of SDS–PAGE gel bands.

Crystallization of pSer111-Rab8A:GDP/GppNHp

Crystallization trials of human pSer111-Rab8A:GDP were performed by the sitting-drop vapour diffusion method, using protein concentrations of 16 mg/ml and a protein:reservoir drop ratio of 1 : 1. Suitably sized crystals were grown in 0.2 M magnesium acetate, 0.1 M sodium cacodylate pH 6.5, 20% PEG 8000. Crystals were cryoprotected in reservoir solution supplemented with 20% glycerol prior to flash freezing in liquid nitrogen. Initial sparse-matrix screening of conditions yielded several hits for pSer111-Rab8A:GppNHp, which failed to produce well-diffracting crystals despite fine-screening efforts. Using numerous crystals grown in 0.1 M MES pH 6.5 and 25% PEG 6000/8000, and in 0.1 M Hepes pH 7.5 and 25% PEG 3000/4000/6000 as seeds, the

method of random microseed matrix seeding [14] was used to produce well-diffracting crystals grown from a protein concentration of 11 mg/ml and a reservoir composed of 0.1 M Tris–HCl pH 8.5, 30% PEG 300. For cryoprotection, a drop of reservoir solution was added to the crystals, which were then maintained in liquid nitrogen.

Diffraction data collection and structure determination

Datasets were collected using synchrotron radiation ($\lambda = 1.0$ Å) at the X06SA-beamline (Swiss Light Source, Villingen, Switzerland). X-ray intensities were assessed and data reduction was carried out with XDS [15]. A dataset for pSer111-Rab8A:GDP was collected from a single crystal, to a resolution of 2.4 Å. For pSer111-Rab8A:GppNHp, partial datasets from two crystals were merged to produce a dataset at 2.5 Å resolution (Table 1). Initial phases were calculated for pSer111-Rab8A:GDP and pSer111-Rab8A:GppNHp by Patterson search procedures using the deposited co-ordinates of Rab8•GDP (PDB ID: 4LHV) and Rab8•GppNHp (PDB ID: 4LHW), respectively [16]. Molecular replacement was carried out using PHASER [17]. Iterative model rebuilding and refinement were performed with COOT [18] and phenix.refine [19], applying non-crystallographic symmetry restraints and Translation/Libration/Screw tensors. Eventually, water molecules were placed automatically using ARP/wARP [20]. The final models of pSer111-Rab8A:GDP (PDB ID: 6STF) and pSer111-Rab8A:GppNHp (PDB ID: 6STG) converged to R_{work}/R_{free} values of 23.3/26.2 and 24.3/27.8. Co-ordinate geometries were confirmed via MOLPROBITY [21] to possess good stereochemistry and small bond-length and angle RMSDs, with no residues lying in the disallowed region of the Ramachandran plot (Table 1).

NMR experiments and analysis

Uniformly ^{15}N labelled Rab1B was expressed and purified as mentioned in the method section, with M9 minimal medium containing $^{15}NH_4Cl$ (1 g/l) as sole nitrogen source. For phosphorylated Rab1B, unlabelled phosphorylated-serine was added to the media since the isotopically labelled derivative is not available. NMR samples were exchanged into final NMR buffer consisting of 20 mM sodium phosphate, 50 mM NaCl, 1 mM DTT, 1 mM MgCl$_2$, pH 6.5 with respective 10 µM GDP or GppNH. 10% ^2H_2O was added for deuterium lock. NMR sample concentrations were 100–300 µM range. Two dimensional-proton ^1H, ^{15}N NMR water-flipback WATERGATE HSQC experiments were recorded on a 600 MHz Bruker NMR spectrometer equipped with a TCI cryoprobe. Experiments were recorded with acquisition times of 122 and 62 ms in the ^1H and ^{15}N dimensions, with a interscan relaxation delay of 1 s. All measurements were performed at 298 K. Proton chemical shifts were calibrated with respect to DSS (2,2-dimethyl-2-silapentane-5-sulfonate), while nitrogen chemical shifts were calibrated indirectly. For data processing, all FID were multiplied with a square-shifted-sine-bell window function and data points with zero-filling before Fourier transformation using the Bruker TOPSPIN3.5pl7 software. Spectra were analyzed using CCPN v.2.4.2 [22].

Cell culture

Flp-In T-Rex HEK293 cells expressing PINK1-3xFLAG were cultured using DMEM (Dulbecco's modified Eagle's medium) supplemented with 10% FBS (foetal bovine serum), 2 mM L-Glutamine, 1× Pen/Strep and 1× non essential amino acids (Life Technologies). Flp-In T-Rex HeLa stable cell lines were cultured in the above mentioned media supplemented with 15 µg/ml of Blasticidin and 100 µg/ml of Hygromycin. Cell transfections of untagged LRRK2 [R1441G], GFP-Rab8A WT or S111A were performed using the Polyethylenimine method [23]. Cultures were induced to express protein by addition of 0.1 µg/ml of doxycycline to the medium for 24 h. To uncouple mitochondria, cells were treated with 10 µM CCCP (Sigma) dissolved in DMSO for 3 h.

Immunoblotting

Samples were subjected to SDS–PAGE and transferred onto nitrocellulose membranes. Membranes were blocked with 5% BSA in TBS-T and incubated at 4°C overnight with the indicated antibodies, diluted in 5% BSA. Membranes for kinase assay screen were incubated with HRP-conjugated secondary antibodies (1 : 10 000) in 5% milk for 1 h at room temperature. Membranes were exposed with ECL substrate. Additional kinase assay immunoblotting membranes were incubated with secondary antibodies, conjugated with LI-COR IRDye in TBS-T (1 : 10 000) and imaged using the LI-COR Odyssey software.

Table 1. Crystallographic data collection and refinement statistics.

	Rab8A:GDP	Rab8A:GppNHp
Crystal parameters		
Space group	C2	P2$_1$
Cell constants	a = 117.6 Å; b = 75.2 Å; c = 107.7 Å; β = 100.5 Å	a = 34.9 Å; b = 93.7 Å; c = 56.1 Å; β = 103.0 Å
Subunits/AU[1]	5	2
Data collection		
Beam line	X06SA, SLS	X06SA, SLS
Wavelength (Å)	1.0	1.0
Resolution range (Å)[2]	50–2.4 (2.5–2.4)	50–2.5 (2.6–2.5)
No. observed reflections	105 949	35 644
No. unique reflections[3]	35 267	11 734
Completeness (%)[2]	97.2 (96.9)	95.9 (92.3)
R_{merge} (%)[2,4]	0.096 (0.574)	0.123 (0.578)
$I/\sigma(I)$[2]	9.5 (2.1)	6.5 (2.0)
Refinement (REFMAC5)		
Resolution range (Å)	30–2.4	30–2.5
No. refl. working set	33 488	11 143
No. refl. test set	1763	586
No. non hydrogen	6875	2845
No. of pSer111	5	2
No. of Mg^{2+}	5	2
No. of nucleotide	5	2
Solvent	45	17
R_{work}/R_{free} (%)[5]	23.3/26.2	24.3/27.8
r.m.s.d. bond (Å)/(°)[6]	0.002/1.2	0.002/1.2
Average B-factor (Å^2)	48.4	51.8
pSer111	89.7	55.1
Nucleotide	40.2	43.4
Ramachandran plot (%)[7]	97.8/2.2/0	98.5/1.5/0
PDB accession code	6STF	6STG

[1]Asymmetric unit;
[2]The values in parentheses for resolution range, completeness, R_{merge} and $I/\sigma(I)$ correspond to the highest resolution shell;
[3]Data reduction was carried out with XDS. Friedel pairs were treated as identical reflections;
[4]$R_{merge}(I) = \Sigma_{hkl}\Sigma_j \mid I(hkl)_j - <I(hkl)> \mid / \Sigma_{hkl} \Sigma_j I(hkl)_j$, where $I(hkl)_j$ is the jth measurement of the intensity of reflection hkl and $<I(hkl)>$ is the average intensity;
[5]$R = \Sigma_{hkl} \mid \mid F_{obs} \mid - \mid F_{calc} \mid \mid / \Sigma_{hkl} \mid F_{obs} \mid$, where R_{free} is calculated for a randomly chosen 5% of reflections, which were not used for structure refinement, and R_{work} is calculated for the remaining reflections;
[6]Deviations from ideal bond lengths/angles;
[7]Percentage of residues in favoured/allowed/outlier region.

Antibodies

The following antibodies were produced by the MRCPPU Reagents and Services at the University of Dundee in sheep: anti-Rab8A phospho-Ser111 (S503D), 4th bleed; raised against residues 104–117 of human Rab8A: RNIEEHApSADVEKMR), Anti-Rab8A pThr72 (S874D), raised against residues 65–79 of human Rab8A:

AGQERFRpTITTAYYR, Anti-Rab1B pSer111 (S817D), 3rd bleed; raised against residues 104–118 of human Rab1B: CQEIDRYApSENVNKLR. Additional phospho-Rab antibodies were produced in development with Abcam: Anti-Rab8A phospho-Thr72 (ab230260 MJFF-20). Anti-Rab8A (D22D8 #6975) was from Cell Signalling Technologies, Anti-6X His Tag antibody (ab18184) from Abcam and Anti-LRRK2 C-terminal (Dardarin clone N241A/34) from NeuroMab. Anti-Rab1B phospho-Thr72 (ABS2131) was from Merck Millipore. Antibodies were used at a final concentration of 1 μg/ml, diluted in 5% BSA.

Results

Identification of MST3 and TAK1 as direct kinases of Rab8A Thr72

Previous biochemical analysis undertaken by our laboratory has demonstrated that PINK1 does not directly phosphorylate Rab GTPases at Ser111 [8]. To search for candidate Rab Ser111-directed kinases, we performed an *in vitro* [γ-^{32}P]-ATP-based screen of ∼140 recombinant kinases against wild-type (WT) or Ser111Ala (S111A) Rab8A in the GDP-bound conformation. We identified multiple kinases capable of phosphorylating wild-type Rab8A *in vitro* as judged by autoradiography including LRRK2 that has been reported to phosphorylate Rab8A at Thr72 (Figure 1A) [10]. Immunoblotting of reactants with a phospho-Ser111-Rab8A (pSer111-Rab8A) antibody did not reveal any kinases that directly phosphorylate GDP-bound Rab8A at Ser111 (Supplementary Figure S1). Consistent with this, we did not identify any kinases that differentially phosphorylate the WT Rab8A more efficiently than the S111A Rab8A mutant (Supplementary Figure S1). We, therefore, repeated the *in vitro* screen with GTP-bound Rab8A, however, under these conditions, we also did not identify any kinase directed towards Ser111 by immunoblotting with a pSer111-Rab8A antibody (Supplementary Figure S2).

Whilst we did not identify the Ser111 kinase in these screens, immunoblotting of reactants with a phospho-Thr72-Rab8A (pThr72-Rab8A) antibody revealed that three kinases, TAK1, MST3 and MAP4K5 were capable of phosphorylating Rab8A at Thr72 equivalent to the LRRK2 site (Figure 1A and Supplementary Figures S1 and S2). Similar to LRRK2, there appeared to be a preference for TAK1 and MST3 to phosphorylate GDP-bound Rab8A compared with GTP-bound Rab8A (Figure 1B and Supplementary Figures S1 and S2). MAP4K5 phosphorylated Thr72 in GDP-bound Rab8A but not GTP-bound Rab8A, however, the overall phosphorylation of Rab8A was unchanged indicating the presence of additional non-Thr72 phosphorylation sites targeted by MAP4K5 *in vitro* (Figure 1A,B and Supplementary Figures S1 and S2). Mutating Thr72 to Ala substantially reduced the phosphorylation of Rab8A by TAK1 and MST3 thereby confirming that this residue represents the major site of phosphorylation (Figure 1C). In contrast there was no reduction in phosphorylation by MAP4K5 indicating that the Thr72 residue is likely to be a minor phosphorylation site (Figure 1C). The screen also identified other kinases including PAK2 and ZAP70 that can efficiently phosphorylate Rab8A (Figure 1A,B and Supplementary Figures S1 and S2) and in future work it would be interesting to determine the site(s) of phosphorylation and understand how these affect Rab8A function.

Phosphorylation of Rabs at Ser111 impairs interactions with Switch II binding regulatory proteins

Upon attachment to their target membranes, Rab GTPases act as molecular switches that are activated by a GEF that catalyzes the exchange of the bound guanosine-5′-diphosphate (GDP) for the more abundant guanosine-5′-triphosphate (GTP). Once active, the GTP-bound Rab can interact with specific effector proteins which mediate a variety of downstream functions including binding to cargoes, enabling vesicle formation and promoting vesicle fusion to target membranes [24]. Rabs are inactivated by GAPs that promote the hydrolysis of GTP to GDP and the inactive Rab is then relocalized to the cytosol [24]. Structural analysis of Rab8A revealed that the PINK1-regulated Ser111 site lies within a short stretch of amino acids within the C-terminal region termed the RabSF3 motif [25] (see Supplementary Figure S3 for a structural depiction of Rab regions and position of Ser111 and Thr72 residues). The RabSF3 motif of Rab8A is close to the Switch II region that mediates GEF binding and we have observed that a Ser111Glu phosphomimetic (S111E) mutant of Rab8A negatively affects its ability to be activated by its cognate GEF, Rabin8 [8]. However, phosphomimetic substitutions often fail to recapitulate the full functional effect of phosphorylation [26].

We, therefore, investigated the effect of the phosphorylation at Ser111 on Rab8A using preparative phosphorylated Rab8A. Employing genetic code expansion technologies for the incorporation of pSer65 into Ubiquitin [13], we were able to produce pSer111-Rab8A in the inactive GDP-bound conformation
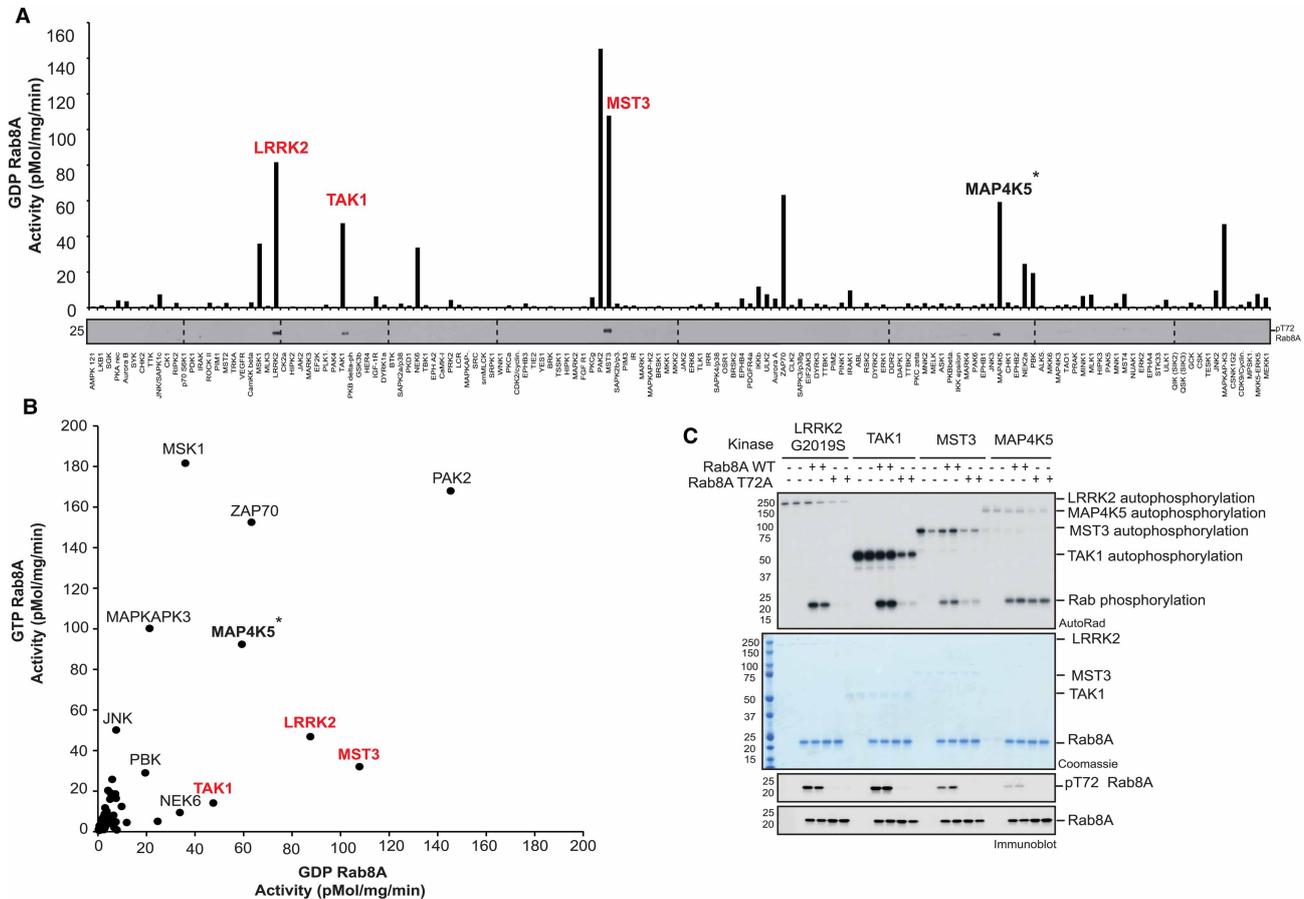
Figure 1. TAK1 and MST3 directly phosphorylate Rab8A at Thr72.

(**A**) Summary analysis of kinase assay screen quantification to identify novel Rab8A kinases. One hundred and forty protein kinases from the MRC PPU Reagents and Services library were assessed for the phosphorylation of GDP-Rab8A. One hundred nanograms of protein kinase was incubated with 2 μg substrate and [γ-^{32}P] ATP for 30 min. Samples were subjected to SDS–PAGE and analysis with Cerenkov counting of Coomassie substrate bands, displayed graphically. Full kinase assay analysis by autoradiography and immunoblotting is described in Supplementary Figure S1. Proteins highlighted in red were identified to phosphorylate Rab8A at Thr72 by phospho-specific immunoblotting. *Thr72 is a minor MAP4K5 phosphorylation site and occurs in GDP-Rab8A but not GTP-Rab8A conformation. (**B**) Correlative analysis of kinase phosphorylation of GTP-Rab8A (y-axis) versus GDP-Rab8A (x-axis). The GTP-Rab8A kinase screen was performed in a similar manner to GDP-Rab8A kinase screen, with full analysis described in Supplementary Figure S2. Kinases that phosphorylate Thr72 as the major site of Rab8A are highlighted in red. (**C**) Mutation of Thr72Ala (T72A) reduces Rab8A phosphorylation by LRRK2, TAK1 and MST3 but not MAP4K5. The indicated kinases were incubated in the presence of WT or T72A GDP-Rab8A. Samples were subjected to SDS–PAGE with analysis by Coomassie staining and [γ-^{32}P] incorporation as visualized by autoradiography and immunoblotting analysis using the indicated antibodies.

(pSer111-Rab8A:GDP) and the active GTP-bound conformation (pSer111-Rab8A:GppNHp) with a yield of 0.15 mg/l of bacterial culture (Supplementary Figure S4). The purity of the proteins was confirmed by SDS–PAGE (Supplementary Figure S4A). Thermal shift analysis demonstrated no significant difference in melting points between pSer111-Rab8A:GDP and WT-Rab8A:GDP or between pSer111-Rab8A:GppNHp and WT-Rab8A:GppNHp suggesting that the pSer111-Rab8A exhibited similar protein stability to the WT-Rab8A (Supplementary Figure S4C). To assess the stoichiometry of phosphorylation, we initially employed Phos-tag™ acrylamide SDS–PAGE to probe for the presence of pSer111-Rab8A:GDP and pSer111-Rab8A:GppNHp relative to the non-phosphorylated (WT) form. Both proteins, pSer111-Rab8A:GDP and pSer111-Rab8A:GppNHp, shifted +10 kDa compared with WT-Rab8A:GDP and WT-Rab8A:GppNHp indicating stoichiometric phosphorylation (Supplementary Figure S4B). LC–MS analysis demonstrated that the mass spectra of pSer111-Rab8A showed the expected increase in molecular mass of +80 Da confirming the presence of a single

phosphorylation (Supplementary Figure S4D). There was no trace of the non-phosphorylated (WT) form in the mass spectra of pSer111-Rab8A, suggesting that the Rab8A protein produced by genetic code expansion was quantitatively phosphorylated (Supplementary Figure S4D).

We next assessed the Switch II-dependent interaction of phosphorylated Rab8A with its GEF and GAP by measuring the nucleotide exchange and GTP hydrolysis rate, respectively. We first compared the Rabin8-mediated GDP–GTP exchange and the TBC1D20-mediated GTP hydrolysis rate in WT-Rab8A and pSer111-Rab8A by measuring the change in their intrinsic Trp fluorescence [27] upon nucleotide exchange over time (Figure 2A,B). We observed an 80% reduction in the GEF activity (Figure 2A,B), and the GAP activity was reduced by ~60% (Figure 2A,B).
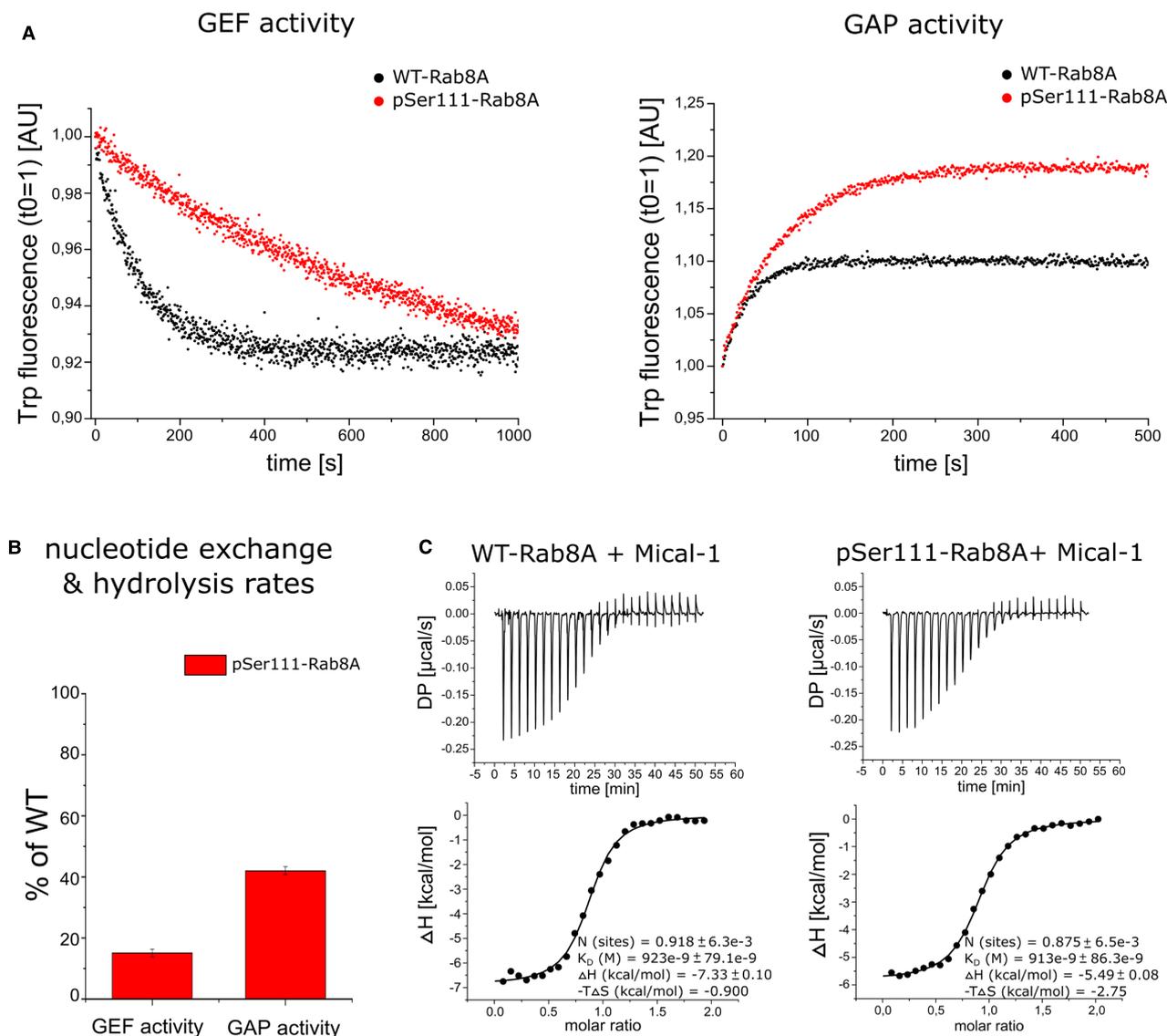
Figure 2. Rab8A Ser111 phosphorylation impairs GEF and GAP interactions.
(**A**) (Left panel) The GDP–GTP exchange catalyzed by the GEF Rabin8 (GEF activity), and the (right panel) GTP hydrolysis catalyzed by the GAP TBC1D20 (GAP activity) were monitored for WT-Rab8A-His6 (black) and pSer111-Rab8A-His6 (red) proteins via intrinsic Trp fluorescence. Data are representative for three independent experiments. (**B**) The nucleotide exchange (GEF activity) and GTP hydrolysis rates (GAP activity) were determined using a single exponential fit, and are represented as percentage of WT. All data ($n = 3$) are represented as mean ± S.D. (**C**) The binding of the effector Mical-1 to WT-Rab8A-His6 and pSer111-Rab8A-His6 was determined by isothermal titration calorimetry (ITC). Data are representative for two independent experiments. The dissociation constants (K_D) for binding affinity are indicated in each graph.

Rab1B shares many structural similarities with Rab8A [25] and can also be phosphorylated in a PINK1-dependent manner in cells at Ser111 equivalent to the Rab8A site (Supplementary Figure S5) [8]. We, therefore, expressed and purified preparative wild-type (WT-Rab1B:GDP/GppNHp) and Ser111-phosphorylated (pSer111-Rab1B:GDP/GppNHp) Rab1B (Supplementary Figure S4A–D). A similar trend was observed for pSer111-Rab1B, whereby the GEF activity was decreased by 60% and the GAP activity by 40% (Supplementary Figure S6).

To determine whether Ser111 phosphorylation was mediating specific effects via the Switch II domain we determined the binding affinity of WT- and pSer111-Rab8A GppNHp-bound forms with the effector Mical-1, which binds outside the Switch II domain [28] (Supplementary Figure S7). Using ITC, we obtained a K_D value of 923 nM for the binding affinity of WT-Rab8A and Mical-1, and a K_D of 913 nM for pSer111 Rab8A with Mical-1, suggesting that the phosphorylation at Ser111 has no effect on Rab8-Mical-1 effector interaction (Figure 2C). The K_D values from the ITC measurements are more than 15 times higher compared with a previous study from Rai et al. [29] characterizing the interaction between WT-Rab8A and Mical-1, which may be due to the C-terminal His$_6$ tag on our WT-Rab8A proteins lowering the binding affinity towards Mical-1. Overall our data suggest that the phosphorylation of Rab8A at Ser111 may influence Switch II-binding by regulators, thus disrupting interactions with its cognate GEF and moderately impairs its interaction with GAPs.

Phosphorylation of Rabs at Ser111 disrupts the ability of LRRK2 to phosphorylate Rabs at Thr72

The LRRK2 kinase has been shown to phosphorylate Rab8A at position Thr72 within the Switch II domain [10], however, the structural determinants and mechanism by which LRRK2 phosphorylates Rabs remained unknown. Since Rab8A Ser111 phosphorylation can disrupt Switch II interactions mediated by Rabin8 and TBC1D20, we next investigated whether Ser111 phosphorylation may impact on LRRK2-mediated phosphorylation of Rab8A at Thr72. To address this we performed an *in vitro* kinase assay using recombinant WT GDP or GTP-bound Rab8A (WT-Rab8A:GDP; WT-Rab8A:GppNHp) or pSer111 GDP or GTP-bound Rab8A (pSer111-Rab8A:GDP; pSer111-Rab8A:GppNHp) incubated with $[\gamma\text{-}^{32}P]$-ATP and an activating LRRK2 mutant [G2019S]. Consistent with previous studies we observed that LRRK2 [G2019S] efficiently phosphorylated WT-Rab8A:GDP but was less able to phosphorylate WT-Rab8A:GppNHp as determined by measuring $[\gamma\text{-}^{32}P]$-ATP incorporation via autoradiography and by immunoblotting of reactants with a pThr72 Rab8A phospho-specific antibody (Figure 3A) [10]. Strikingly, we found that the ability of LRRK2 [G2019S] to phosphorylate pSer111-Rab8A:GDP was disrupted (compared with WT-Rab8A:GDP) and a similar reduction was determined for pSer111-Rab8A:GppNHp (compared with WT-Rab8A:GppNHp) (Figure 3A). This was not due to inhibition of LRRK2 catalytic activity since LRRK2 autophosphorylation was unchanged (Figure 3A). In agreement with previous results, LRRK2 phosphorylates Rab1B *in vitro* at Thr72 equivalent to the Rab8A Thr72 site [10]. To determine whether the effect of Ser111 phosphorylation was more generalizable to other LRRK2 Rab substrates that are common to PINK1, we next assessed the ability of LRRK2 [G2019S] to phosphorylate Rab1B *in vitro*. Similar to Rab8A, we observed a significant reduction in the ability of LRRK2 [G2019S] to phosphorylate pSer111-Rab1B:GDP or pSer111-Rab1B:GppNHp (compared with WT-Rab1B) as judged by autoradiography and immunoblotting of reactants with a p-Thr72 Rab1B phospho-specific antibody (Supplementary Figure S8A).

We next compared the ability of other Rab Thr72-directed kinases, MST3 and TAK1, to phosphorylate pSer111 Rab8A. We performed a side-by-side comparison of the efficiency of phosphorylation of WT-Rab8A:GDP or pSer111-Rab8A:GDP by LRRK2, MST3 and TAK1 (Figure 3B). Indeed pSer111-Rab8A:GDP reduced LRRK2-mediated phosphorylation compared with WT-Rab8A:GDP. In contrast, MST3 and TAK1 were still capable of phosphorylating pSer111-Rab8A:GDP to a similar extent as WT-Rab8A:GDP (Figure 3B). Consistent with these results we found pSer111-Rab1B:GDP has no effect on the ability of MST3 and TAK1 kinases to phosphorylate Thr72 compared with WT-Rab1B:GDP compared with LRRK2 (Supplementary Figure S8B).

Phosphorylation at Ser111 does not induce major structural changes in Rab8A and Rab1B

To understand the mechanism by which Ser111 phosphorylation impacts on its interactions with its GEF, GAP and LRRK2, we solved the structure of pSer111-Rab8A. We were able to obtain well-diffracting crystals for
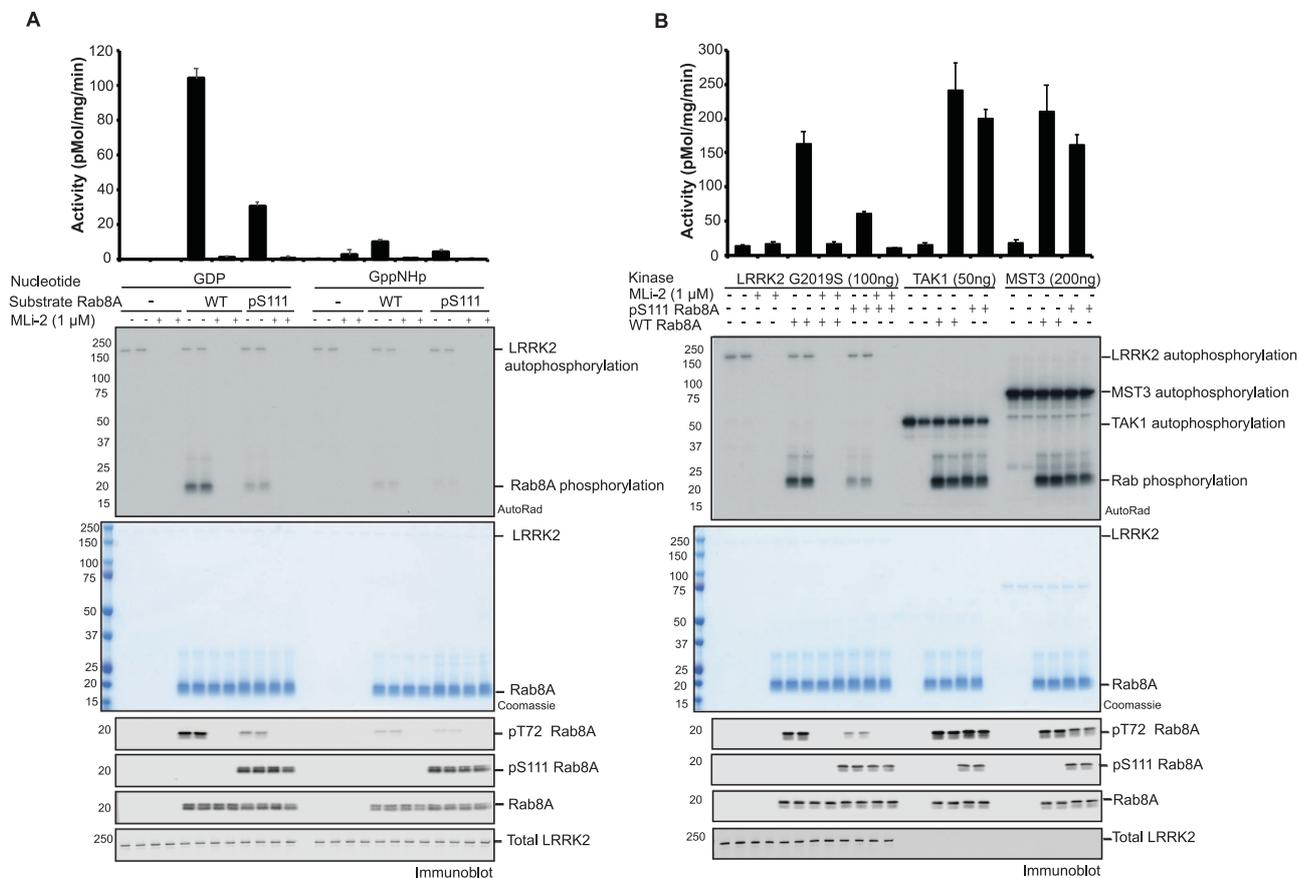
Figure 3. Rab8A Ser111 phosphorylation disrupts LRRK2-mediated Thr72 phosphorylation *in vitro*.

A) 100 ng of recombinant LRRK2 [G2019S] protein was incubated with [γ-^{32}P] and 2 μg of WT or pSer111 Rab8A, in either the GDP or GTP (GppNHp) bound conformation, in the absence or presence of the LRRK2 inhibitor, MLi-2 for 30 min. Samples were subjected to SDS–PAGE, and analyzed by either Coomassie staining, [γ-^{32}P] incorporation measured by autoradiography with Cerenkov counting (top panel) and immunoblot analysis, using the indicated antibodies (lower panel). Results are means ±S.E.M. (*n* = 4). (**B**) Thr72 specific kinases were assessed for phosphorylation of GDP bound WT or pSer111 Rab8A. 100 ng of LRRK2 G2019S, 50 ng TAK1 or 200 ng MST3 were incubated with 2 μg substrate using identical conditions and analysis as in (**A**).

both pSer111-Rab8A:GDP (2.4 Å resolution, R_{free} = 26.2%, PDB ID: 6STF) and pSer111-Rab8A:GppNHp (2.5 Å resolution, R_{free} = 27.8%, PDB ID: 6STG) (Table 1; see Figure 4 and Supplementary Figure S9 for representative depictions of the electron density). Phosphorylated Rab8A exhibits a typical small GTPase fold [30,31] with highly flexible Switch regions in the GDP-bound form, and well-defined structured Switch regions in the GppNHp-bound form (Figure 4). The pSer111 residue is located C-terminal of helix α3 in a loop above the Switch II region (α2). The superimposed structures of pSer111-Rab8A and WT-Rab8A [16] showed that the phosphorylation at Ser111 does not impact the overall structure of Rab8A (Figure 4 and Supplementary Figure S9). Interestingly, the formation of a new intramolecular interaction between the phosphate group and the side chain of Arg79 at the C-terminal end of Switch II is striking in the structure of pSer111-Rab8A:GDP (Figure 4 and Supplementary Figure S9). Nevertheless, the spatial proximity of pSer111 to the Switch II region (α2) could allow for dynamic interactions between pSer111 and residues within Switch II. To test the potential conformational consequences of Ser111 phosphorylation, we performed nuclear magnetic resonance experiments to compare the phosphorylated and non-phosphorylated forms. However, since we were unable to produce isotopically labelled phosphorylated Rab8A, we instead produced the close homologue Rab1B as a surrogate (Supplementary Figure S10). When comparing the ^{1}H ^{15}N Heteronuclear Single Quantum Coherence (HSQC) NMR data for wild-type and Ser111-phosphorylated Rab1B in the GDP and GppNHp states, most of the chemical shifts overlap well, indicating that Ser111 phosphorylation, probably does not lead to major
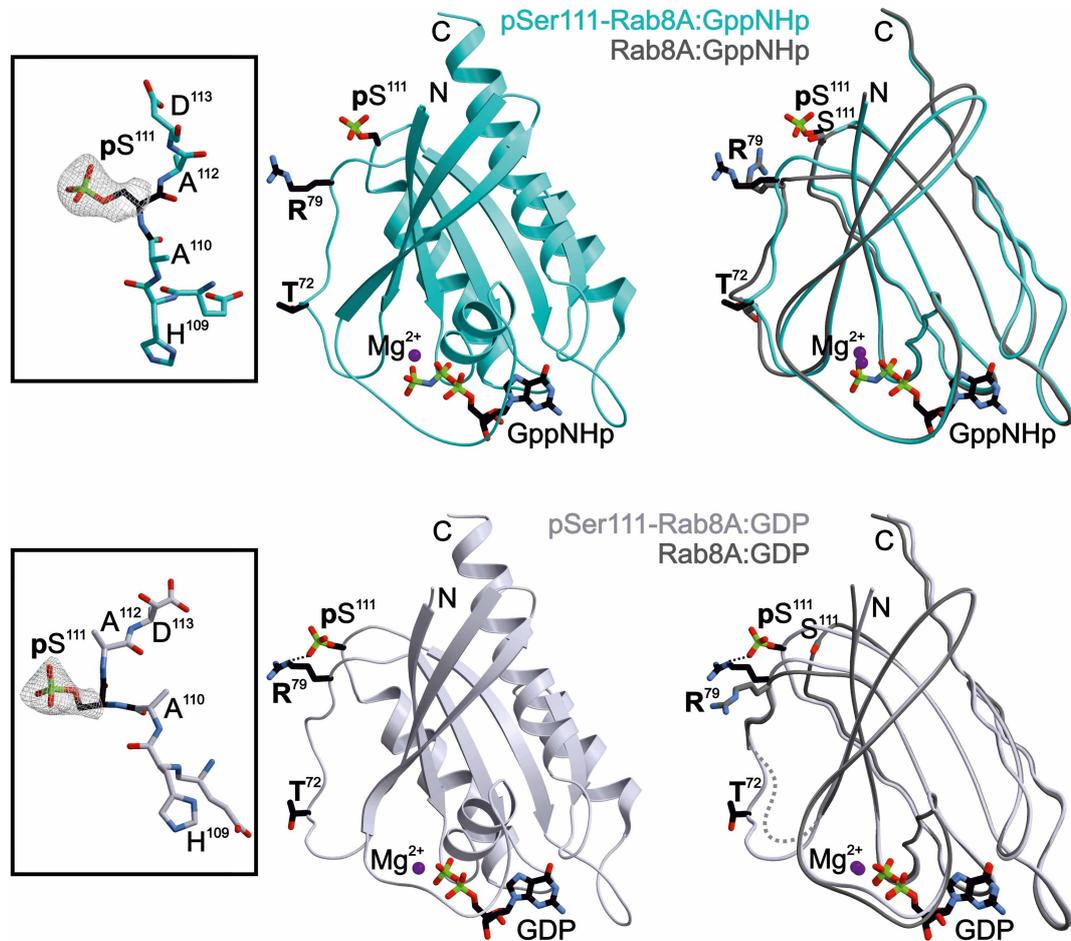
Figure 4. Model of the X-ray structure of Rab8A phosphorylated at Ser111.

Centre: ribbon drawings of active pSer111-Rab8A:GppNHp (PDB ID 6STG, cyan, upper panel) and inactive pSer111-Rab8A: GDP proteins (PDB ID 6STF, lavender, lower panel), respectively. pSer111 and nucleotides are shown as stick models. Left: the inset depicts the $2F_o–F_c$ electron density map of the pSer111 side chain. The surrounding peptide sequence is presented as stick model. Right: the panel displays the overlay of the phosphorylated Ser111-Rab8A structure with its unmodified counterparts (Rab8A:GppNHp, PDB ID 4LHW; Rab8A:GDP, PDB ID 4LHV) [16]. Purple sphere: Mg^{2+}. An intramolecular salt bridge formed between pSer111 and Arg79 in pSer111-Rab8A:GDP is indicated with a dotted line.

structural alterations on Rab1B in solution. However, some of the resonances show shifts because of a change in the chemical environment close to the phosphate group (Supplementary Figure S11). Overall, the lack of conformational changes observed in the crystal structures (pSer111-Rab8A) are consistent with the lack of structural changes seen in solution (pSer111-Rab1B). In future work it would be interesting to elucidate the structure of Rab1B in complex with its effectors to determine how pSer111 might alter the interaction between the Switch II region and known Rab1B regulators such as the GEF, as well as LRRK2.

Evidence of interplay of PINK1 and LRRK2 signalling on Rab8A in cells

Under basal conditions in which PINK1 is inactive, Rab8A is phosphorylated by LRRK2. Previous studies have demonstrated that the hyperactive mutant LRRK2 [R1441G] leads to increased Rab8A Thr72 phosphorylation [9,10]. Under mitochondrial depolarization that can be induced by mitochondrial uncouplers, (e.g. CCCP) PINK1 is stabilized and activated and can phosphorylate Rab8A at Ser111 [8]. We, therefore, expressed LRRK2 [R1441G], and wild-type as well as a non-phosphorylatable S111A mutant of GFP-Rab8A in HEK 293 Flp-In TREx cells that express PINK1-3xFLAG. Cells were pre-treated with DMSO or 100 nM MLi-2 (LRRK2

inhibitor) for 1.5 h followed by either 10 μM CCCP or DMSO control for 3 h. Cells were lysed and whole cell extracts analyzed by immunoblotting with anti-GFP, and anti-LRRK2 antibodies that confirmed uniform expression across all conditions (Supplementary Figure S12). Immunoblotting with anti-PINK1 antibodies and OPA1 antibodies confirmed equivalent expression across basal and mitochondrial depolarized conditions (Supplementary Figure S12). To visualize phosphorylated Rab8A, we undertook Phos-tag™ SDS–PAGE and immunoblotting with anti-GFP antibody, demonstrating a single electrophoretic band shift of ∼40% total Rab8A under basal conditions that was abolished by MLi-2 treatment indicating LRRK2-mediated Thr72 phosphorylation (Figure 5 and Supplementary Figure S12). Furthermore, these findings were confirmed by an anti-phospho-Rab8A-Thr72 antibody (Figure 5 and Supplementary Figure S12). Upon combined treatment of MLi-2 and CCCP, we observed the appearance of a single electrophoretic band of ∼20% Rab8A due to PINK1-mediated Ser111 phosphorylation that migrated at a similar pattern to LRRK2-mediated monophosphorylated Rab8A and was also positively detected by the anti-phospho-Rab8A-Ser111 antibody (Figure 5 and Supplementary Figure S12). Upon removal of MLi-2 and in the presence of CCCP, we observed a double electrophoretic band shift with the upper band representing the dual phosphorylated Rab8A as confirmed by immunoblotting of the Phos-tag™ gel with anti-phospho-Rab8A-Thr72 and anti-phospho-Rab8A-Ser111
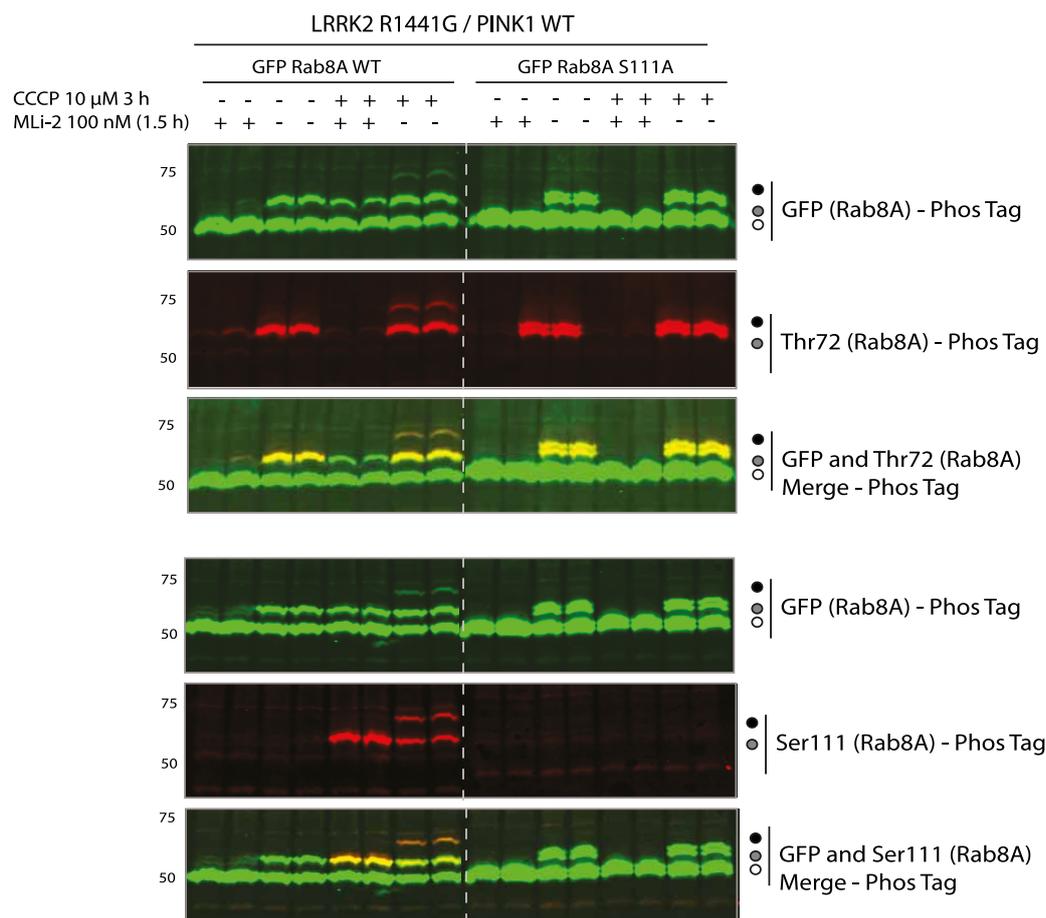

Figure 5. PINK1 and LRRK2 signalling converge on Rab8A in cells.
HEK293 Flp-In TREx cells stably expressing PINK1-3XFLAG were co-transfected with 9 μg of LRRK2 R1441G and 3 μg of GFP Rab8A WT or S111A. Cells were treated with DMSO, 100 nM MLi-2 (1.5 h), 10 μM CCCP (3 h) or a combination of each. Cells were lysed and underwent Phos-tag analysis with total and phospho-specific antibodies using the LI-COR Odyssey imaging system for detection. IRDye 800CW fluorescent secondary antibody was utilized for GFP Rab total signal, whilst IRDye 680RW fluorescent antibody was used for the specific phospho-Rab detection. The presence of yellow fluorescence upon multiplexing with Image Studio software, indicates the presence of site-specific phosphorylated Rab within the GFP total Rab population.

antibodies (Figure 5 and Supplementary Figure S12). However, quantification of the immunoblot signals by LI-COR (Supplementary Figure S13A–C) revealed that the double phosphorylated species represents only 2% of the total Rab which is less than predicted (4.5%) (Supplementary Figure S13C) based on Ser111-monophosphorylation levels (Supplementary Figure S13A,B) and suggests that pThr72 is preferentially incorporated into unmodified Rab8A rather than Ser111-phosphorylated Rab8A consistent with our *in vitro* studies (Figure 5). The interplay between PINK1 and LRRK2 is not observed in cells expressing the PINK1 kinase-inactive D384A mutation highlighting that cross-talk of PINK1 and LRRK2 signalling is mediated by PINK1 catalytic activity (Supplementary Figure S14).

Discussion

Using genetic code expansion technology, we have been able to demonstrate that PINK1-dependent phosphorylation of Rab GTPases at Ser111 impairs the ability of Rabs to interact with GEFs and GAPs. Interference of the GEF or GAP binding would trap the phosphorylated Rab protein in either the inactive GDP- or active GTP-bound state (Figure 2 and Supplementary Figure S6). Furthermore, we have also found that PINK1-dependent Rab phosphorylation blocks the ability of the LRRK2 kinase but not TAK1 or MST3 to phosphorylate Thr72 (Figures 3 and 6; Supplementary Figure S8).

The Ser111 residue lies within a C-terminal α3/β5 loop of Rab8A, that connects the α helix 3 with the β sheet 5 known as the SF3 motif and is adjacent to the Switch II domain (Figure 4) [32,33]. The Switch II region represents the major interaction surface for Rab effectors and undergoes dynamic conformational change upon alteration between its GTP and GDP-bound forms [25]. Across all Rab proteins in their active state, there is structural heterogeneity both within the Switch domains, and also the SF3 motif (with little change in other regions) explaining how different Rab proteins can bind to specific sets of effector proteins to regulate distinct pathways [34–36]. Previous studies have reported a role for the SF3 motif in selective recruitment of effectors via direct effector-specific contact sites e.g. the recruitment of Rabphillin by Rab3a via SF3 motif binding sites [32]. However, the role of post translational modifications including phosphorylation within the SF3 motif on effector interactions has not been studied with preparative amounts of modified Rab proteins.

The phosphorylation at Ser111 did not induce any major changes in the structure of Rab8A (Figure 4 and Supplementary Figure S9), nor in Rab1B (Supplementary Figures S10 and S11), despite impacting on GEF/GAP interactions (Figure 2A,B and Supplementary Figure S6). The effect of pSer111 on Rabin8-mediated nucleotide exchange is similar in extent to the phosphomimetic S111E-Rab8A mutant, suggesting that the introduction of negative charges within the SF3 motif may influence GEF/GAP binding [8]. Consistent with this possibility, the Rab8A:Rabin8 structure has recently been analyzed using molecular dynamics simulation revealing a salt-bridge interaction between residue Asp187 of Rabin8 with Arg79 that lies within the Switch II domain of Rab8A [37]. This is consistent with the observation that an intramolecular H-bond is created by the presence of the phosphate at Ser111 with the side chain of Arg79 (Figure 4 and Supplementary Figure S9). Ser111 is located opposite a negative surface patch of Rabin8 in proximity to Asp187. Thus addition of a negative charge at Ser111 either by S111E or pSer111 disrupts the interaction between Asp187 of Rabin8 and Arg79 of the Rab8A [37]. Whilst the Arg79 residue is not part of the TBC1D20 binding site in Rab8A its close distance might explain why the pSer111-effect is not as pronounced for the GAP TBC1D20 as for the Rabin8 interaction (Figure 2A,B and Supplementary Figure S7). Furthermore, we did not detect any influence of Ser111 phosphorylation on the interaction with the effector Mical-1 because the Switch II region (α2) of Rab8A is not part of the Mical-1 binding site (Supplementary Figure S7). Arg79 is conserved in Rab1B, and isotope labelling methods such as NMR of the pSer111-Rab1B:GEF in comparison with WT Rab1B:GEF are envisioned to study the central role of Arg79 in mediating polar interactions between Rab1B and effectors. In addition the role of Arg79 in mediating specific polar interactions between Rab8A/Rab1B and LRRK2 that is distinct from those of with MST3 or TAK1 will be addressed.

There is great interest in whether the PINK1 signalling pathway converges with other PD gene pathways and whether there are critical signalling nodes mediating neurodegeneration in PD. Few studies have suggested a link between PINK1 and LRRK2 indicating that LRRK2 kinase activity may inhibit PINK1 induced mitophagy [38]. Our data suggest that PINK1-dependent signalling may converge with LRRK2 signalling at Rab8A (Figure 3 and Supplementary Figure S8) and the antagonistic interplay between Ser111 phosphorylation and Thr72 phosphorylation is genetically concordant with how respective mutations in PINK1 and LRRK2 cause PD (Figure 6). We could show that LRRK2 preferentially phosphorylated GDP-bound Rab8A compared with GTP-bound Rab8A, which has not been observed in cells where LRRK2 exclusively phosphorylates the
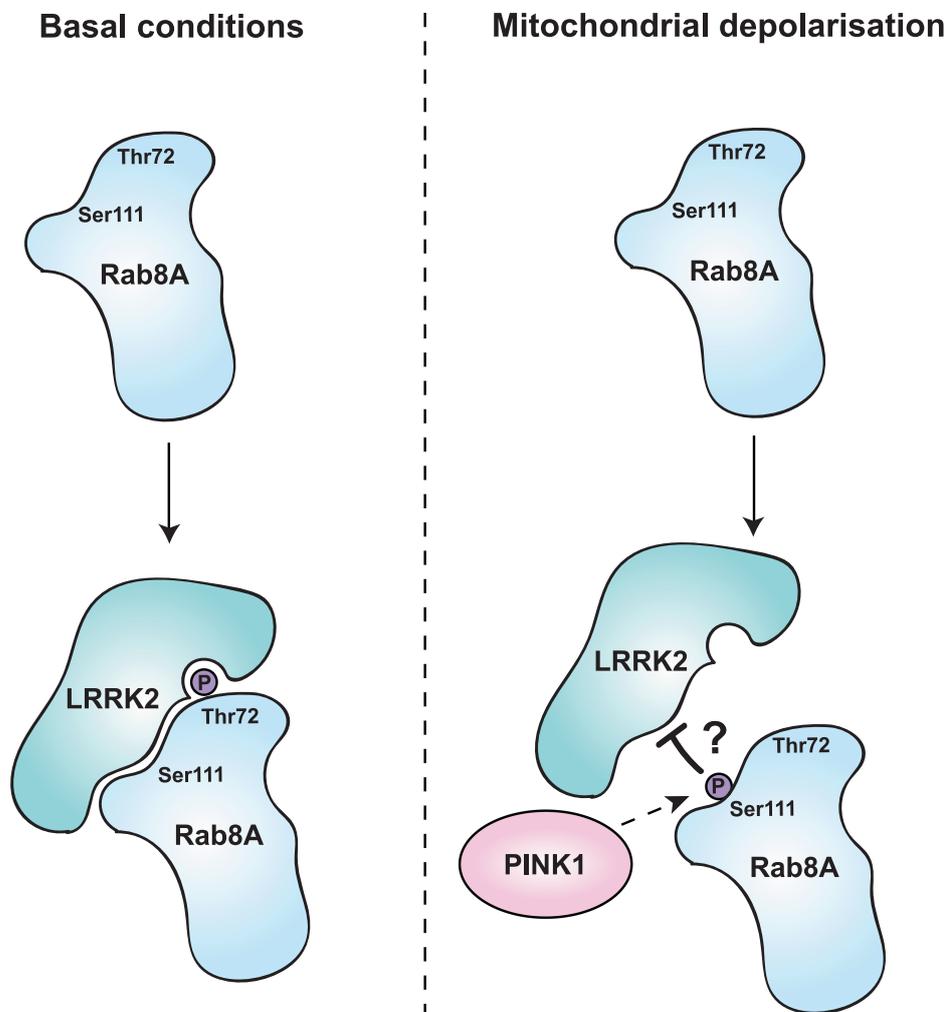
Figure 6. Schematic model of PINK1 and LRRK2 interplay converging on Rab8A.
Indirect phosphorylation of Rab8A at Ser111, reduces the ability of LRRK2 to interact and phosphorylate residue Thr72.

GTP-bound Rab8A [39]. There is so far no structural explanation to this and in the future it will be important to study the authentic membrane-tethered Rab8A. Endogenous phosphorylation of Thr72 by LRRK2 is low, which hampers the ability to assess the interplay of PINK1 and LRRK2 phosphorylation of Rabs. Interestingly, recent studies revealed that effectors including RILPL1 and RILPL2 bind preferentially to LRRK2-phosphorylated Rab Thr72 and this leads to inhibition of primary cilia in the brains of mice harbouring the hyperactive LRRK2 [R1441G] mutation [26]. Hence it is important to analyze if cilia inhibition by LRRK2 is regulated by PINK1 *in vivo* performing a comparative analysis of LRRK2 [R1441G]/PINK1 knockout double mutant mice with littermate controls. Whilst LRRK2 has been mainly implicated in lysosomal biology, there is increasing evidence that LRRK2 mutations are associated with mitochondrial dysfunction [40] and in future work it will be interesting to explore whether this is via a cross-talk between PINK1-regulated Rabs and mitochondrial homeostasis.

Our analysis revealed that many other kinases can regulate Rab phosphorylation including MST3 and TAK1 that are Thr72-directed kinases and MSK1, ZAP70, PAK2, MAP4K5, MAPKAPK3, JNK, PBK, TAK1 and NEK6 whose sites of Rab phosphorylation are unknown. TAK1 has previously been shown to phosphorylate Thr72 in Rab1 and this is important for immunity against Legionella infection [41]. Our studies suggest that the mechanism by which LRRK2 phosphorylates Rab Thr72 is distinct from MST3 and TAK1. To date cellular analysis has not suggested an interplay between TAK1 or MST3 with LRRK2 in the Rab-regulation via Thr72 suggesting that this signalling cascade may be distinct from that of LRRK2 biology. However, the discovery of

MST3 and TAK1 as Rab8A Thr72 kinases represent new tools to enzymatically purify preparative amounts of Thr72 phosphorylated Rab8A which will accelerate LRRK2 directed research into understanding the consequence of Thr72 phosphorylation on regulation by effectors.

In conclusion, our studies have revealed an important role for PINK1-dependent phosphorylation of the SF3 motif of Rabs in the regulation of effector interactions including an antagonistic interplay with LRRK2-mediated Thr72 phosphorylation within the Switch II region (Figure 6). In future studies, it will be important to identify the upstream direct kinase for Ser111 which might have therapeutic potential to act as a brake on LRRK2-mediated Thr72 phosphorylation.

Whilst this article has been in the preprint phase, two studies have applied our findings of MST3 to express homogenous amounts of phosphorylated Thr72-Rab8A for biochemical and structural studies [42,43].

Accession codes

Structure factors and co-ordinates for pSer111-Rab8A:GDP and pSer111-Rab8A:GppNHp were deposited in the RCSB Protein Data Bank (PDB) under the accession codes 6STF and 6STG, respectively.

Competing Interests

The authors declare that there are no competing interests associated with the manuscript.

Funding

Author Contributions

S.V. and K.M. performed most of the experiments. B.B. and M.G. performed x-ray crystallography; and N.K. performed NMR analysis under the supervision of MS. Y.-C.L. contributed to *in vitro* kinase screening and validation. R.T. generated cDNA constructs used in the project. I.V. and P.K.S. contributed to cell-based experiments. S.V., K.M., B.B., M.G., N.K., M.S., A.I. and M.M.K.M. planned experiments and analyzed results. M.M.K.M. and A.I. wrote the paper with contribution from all the authors. M.M.K.M. and A.I. conceived and supervised the project.

Acknowledgements

Abbreviations

CCCP, carbonyl cyanide m-chlorophenyl hydrazone; GAP, GTPase activating protein; GEF, guanine nucleotide exchange factor; PD, Parkinson's disease; PINK1, PTEN-induced kinase 1; pSer, phospho-serine; TSA, thermal shift assay.

References

1　Valente, E.M., Abou-Sleiman, P.M., Caputo, V., Muqit, M.M.K., Harvey, K., Gispert, S. et al. (2004) Hereditary early-onset Parkinson's disease caused by mutations in PINK1. *Science* **304**, 1158–1160 https://doi.org/10.1126/science.1096284

2　Kondapalli, C., Kazlauskaite, A., Zhang, N., Woodroof, H.I., Campbell, D.G., Gourlay, R. et al. (2012) PINK1 is activated by mitochondrial membrane potential depolarization and stimulates Parkin E3 ligase activity by phosphorylating Serine 65. *Open Biol.* **2**, 120080 https://doi.org/10.1098/rsob.120080

3   Shiba-Fukushima, K., Imai, Y., Yoshida, S., Ishihama, Y., Kanao, T., Sato, S. et al. (2012) PINK1-mediated phosphorylation of the Parkin ubiquitin-like domain primes mitochondrial translocation of Parkin and regulates mitophagy. *Sci. Rep.* **2**, 1002 https://doi.org/10.1038/srep01002

4   Kane, L.A., Lazarou, M., Fogel, A.I., Li, Y., Yamano, K., Sarraf, S.A. et al. (2014) PINK1 phosphorylates ubiquitin to activate Parkin E3 ubiquitin ligase activity. *J. Cell Biol.* **205**, 143–153 https://doi.org/10.1083/jcb.201402104

5   Kazlauskaite, A., Kondapalli, C., Gourlay, R., Campbell, D.G., Ritorto, M.S., Hofmann, K. et al. (2014) Parkin is activated by PINK1-dependent phosphorylation of ubiquitin at Ser65. *Biochem. J.* **460**, 127–139 https://doi.org/10.1042/BJ20140334

6   Koyano, F., Okatsu, K., Kosako, H., Tamura, Y., Go, E., Kimura, M. et al. (2014) Ubiquitin is phosphorylated by PINK1 to activate parkin. *Nature* **510**, 162–166 https://doi.org/10.1038/nature13392

7   Ordureau, A., Sarraf Shireen, A., Duda, D.M., Heo, J.-M., Jedrychowski, M.P., Sviderskiy, V.O. et al. (2014) Quantitative proteomics reveal a feedforward mechanism for mitochondrial PARKIN translocation and ubiquitin chain synthesis. *Mol. Cell* **56**, 360–375 https://doi.org/10.1016/j.molcel.2014.09.007

8   Lai, Y.C., Kondapalli, C., Lehneck, R., Procter, J.B., Dill, B.D., Woodroof, H.I. et al. (2015) Phosphoproteomic screening identifies Rab GTPases as novel downstream targets of PINK1. *EMBO J.* **34**, 2840–2861 https://doi.org/10.15252/embj.201591593

9   Steger, M., Diez, F., Dhekne, H.S., Lis, P., Nirujogi, R.S., Karayel, O. et al. (2017) Systematic proteomic analysis of LRRK2-mediated Rab GTPase phosphorylation establishes a connection to ciliogenesis. *eLife* **6**, e31012 https://doi.org/10.7554/eLife.31012

10   Steger, M., Tonelli, F., Ito, G., Davies, P., Trost, M., Vetter, M. et al. (2016) Phosphoproteomics reveals that Parkinson's disease kinase LRRK2 regulates a subset of Rab GTPases. *eLife* **5**, e12813 https://doi.org/10.7554/eLife.12813

11   Mir, R., Tonelli, F., Lis, P., Macartney, T., Polinski, N.K., Martinez, T.N. et al. (2018) The Parkinson's disease VPS35[D620N] mutation enhances LRRK2-mediated Rab protein phosphorylation in mouse and human. *Biochem. J.* **475**, 1861–1883 https://doi.org/10.1042/BCJ20180248

12   Fell, M.J., Mirescu, C., Basu, K., Cheewatrakoolpong, B., DeMong, D.E., Ellis, J.M. et al. (2015) MLi-2, a potent, selective, and centrally active compound for exploring the therapeutic potential and safety of LRRK2 kinase inhibition. *J. Pharmacol. Exp. Ther.* **355**, 397–409 https://doi.org/10.1124/jpet.115.227587

13   Rogerson, D.T., Sachdeva, A., Wang, K., Haq, T., Kazlauskaite, A., Hancock, S.M. et al. (2015) Efficient genetic encoding of phosphoserine and its nonhydrolyzable analog. *Nat. Chem. Biol.* **11**, 496–503 https://doi.org/10.1038/nchembio.1823

14   Shaw Stewart, P.D., Kolek, S.A., Briggs, R.A., Chayen, N.E. and Baldock, P.F.M. (2011) Random microseeding: a theoretical and practical exlporation of seed stability and seeding techniques for successful protein crystallisation. *Cryst. Growth Des.* **11**, 3432–3441 https://doi.org/10.1021/cg2001442

15   Kabsch, W. (2010) Integration, scaling, space-group assignment and post-refinement. *Acta Crystallogr. D Biol. Crystallogr.* **66**(Pt 2), 133–144. https://doi.org/10.1107/S0907444909047374

16   Guo, Z., Hou, X., Goody, R.S. and Itzen, A. (2013) Intermediates in the guanine nucleotide exchange reaction of Rab8 protein catalyzed by guanine nucleotide exchange factors Rabin8 and GRAB. *J. Biol. Chem.* **288**, 32 466–32 474 https://doi.org/10.1074/jbc.M113.498329

17   McCoy, A.J., Grosse-Kunstleve, R.W., Adams, P.D., Winn, M.D., Storoni, L.C. and Read, R.J. (2007) *Phaser* crystallographic software. *J. Appl. Crystallogr.* **40**(Pt 4), 658–674. https://doi.org/10.1107/S0021889807021206

18   Emsley, P. and Cowtan, K. (2004) *Coot*: model-building tools for molecular graphics. *Acta Crystallogr. D Biol. Crystallogr.* **60**(Pt 12 Pt 1), 2126–2132 https://doi.org/10.1107/S0907444904019158

19   Adams, P.D., Afonine, P.V., Bunkóczi, G., Chen, V.B., Davis, I.W., Echols, N. et al. (2010) *PHENIX*: a comprehensive Python-based system for macromolecular structure solution. *Acta Crystallogr. D Biol. Crystallogr.* **66**(Pt 2), 213–221. https://doi.org/10.1107/S0907444909052925

20   Langer, G., Cohen, S.X., Lamzin, V.S. and Perrakis, A. (2008) Automated macromolecular model building for X-ray crystallography using ARP/wARP version 7. *Nat. Protoc.* **3**, 1171–1179 https://doi.org/10.1038/nprot.2008.91

21   Chen, V.B., Arendall, W.B., Headd, J.J., Keedy, D.A., Immormino, R.M., Kapral, G.J. et al. (2010) *Molprobity*: all-atom structure validation for macromolecular crystallography. *Acta Crystallogr. D Biol. Crystallogr.* **66**(Pt 1), 12–21. https://doi.org/10.1107/S0907444909042073

22   Vranken, W.F., Boucher, W., Stevens, T.J., Fogh, R.H., Pajon, A., Llinas, M. et al. (2005) The CCPN data model for NMR spectroscopy: development of a software pipeline. *Proteins* **59**, 687–696 https://doi.org/10.1002/prot.20449

23   Reed, S.E., Staley, E.M., Mayginnes, J.P., Pintel, D.J. and Tullis, G.E. (2006) Transfection of mammalian cells using linear polyethylenimine is a simple and effective means of producing recombinant adeno-associated virus vectors. *J. Virol. Methods* **138**, 85–98 https://doi.org/10.1016/j.jviromet.2006.07.024

24   Pylypenko, O., Hussein, H., Yu, I.-M. and Houdusse, A. (2018) Rab GTPases and their interacting protein partners: Structural insights into Rab functional diversity. *Small GTPases* **9**, 22–48 https://doi.org/10.1080/21541248.2017.1336191

25   Müller, M.P. and Goody, R.S. (2018) Molecular control of Rab activity by GEFs, GAPs and GDI. *Small GTPases* **9**, 5–21 https://doi.org/10.1080/21541248.2016.1276999

26   Dhekne, H.S., Yanatori, I., Gomez, R.C., Tonelli, F., Diez, F., Schüle, B. et al. (2018) A pathway for Parkinson's disease LRRK2 kinase to block primary cilia and sonic hedgehog signaling in the brain. *eLife* **7**, e40202 https://doi.org/10.7554/eLife.40202

27   Müller, M.P., Shkumatov, A.V., Oesterlin, L.K., Schoebel, S., Goody, P.R., Goody, R.S. et al. (2012) Characterization of enzymes from *legionella pneumophila* involved in reversible adenylylation of Rab1 protein. *J. Biol. Chem.* **287**, 35 036–35 046 https://doi.org/10.1074/jbc.M112.396861

28   Vanoni, M.A. (2017) Structure-function studies of MICAL, the unusual multidomain flavoenzyme involved in actin cytoskeleton dynamics. *Arch. Biochem. Biophys.* **632**, 118–141 https://doi.org/10.1016/j.abb.2017.06.004

29   Rai, A., Oprisko, A., Campos, J., Fu, Y., Friese, T., Itzen, A. et al. (2016) bMERB domains are bivalent Rab8 family effectors evolved by gene duplication. *eLife* **5**, e18675 https://doi.org/10.7554/eLife.18675

30   Schlichting, I., Almo, S.C., Rapp, G., Wilson, K., Petratos, K., Lentfer, A. et al. (1990) Time-resolved X-ray crystallographic study of the conformational change in Ha-Ras p21 protein on GTP hydrolysis. *Nature* **345**, 309–315 https://doi.org/10.1038/345309a0

31   Stenmark, H. and Olkkonen, V.M. (2001) The Rab GTPase family. *Genome Biol.* **2**, REVIEWS3007 https://doi.org/10.1186/gb-2001-2-5-reviews3007

32   Ostermeier, C. and Brunger, A.T. (1999) Structural basis of Rab effector specificity: crystal structure of the small G protein Rab3A complexed with the effector domain of rabphilin-3A. *Cell* **96**, 363–374 https://doi.org/10.1016/S0092-8674(00)80549-8

33   Pereira-Leal, J.B. and Seabra, M.C. (2000) The mammalian Rab family of small GTPases: definition of family and subfamily sequence motifs suggests a mechanism for functional specificity in the Ras superfamily. *J. Mol. Biol.* **301**, 1077–1087 https://doi.org/10.1006/jmbi.2000.4010

34   Hutagalung, A.H. and Novick, P.J. (2011) Role of Rab GTPases in membrane traffic and cell physiology. *Physiol. Rev.* **91**, 119–149 https://doi.org/10.1152/physrev.00059.2009

35   Pfeffer, S. and Aivazian, D. (2004) Targeting Rab GTPases to distinct membrane compartments. *Nat. Rev. Mol. Cell Biol.* **5**, 886–896 https://doi.org/10.1038/nrm1500

36   Wu, Y.W., Oesterlin, L.K., Tan, K.-T., Waldmann, H., Alexandrov, K. and Goody, R.S. (2010) Membrane targeting mechanism of Rab GTPases elucidated by semisynthetic protein probes. *Nat. Chem. Biol.* **6**, 534–540 https://doi.org/10.1038/nchembio.386

37   Pourjafar-Dehkordi, D., Vieweg, S., Itzen, A. and Zacharias, M. (2019) Phosphorylation of Ser111 in Rab8a modulates Rabin8-dependent activation by perturbation of side chain interaction networks. *Biochemistry* **58**, 3546–3554 https://doi.org/10.1021/acs.biochem.9b00516

38   Bonello, F., Hassoun, S.-M., Mouton-Liger, F., Shin, Y.S, Muscat, A., Tesson, C. et al. (2019) LRRK2 impairs PINK1/Parkin-dependent mitophagy via its kinase activity: pathologic insights into Parkinson's disease. *Hum. Mol. Genet.* **28**, 1645–1660 https://doi.org/10.1093/hmg/ddz004

39   Liu, Z., Bryant, N., Kumaran, R., Beilina, A., Abeliovich, A., Cookson, M.R. et al. (2018) LRRK2 phosphorylates membrane-bound rabs and is activated by GTP-bound Rab7L1 to promote recruitment to the trans-Golgi network. *Hum. Mol. Genet.* **27**, 385–395 https://doi.org/10.1093/hmg/ddx410

40   Singh, A., Zhi, L. and Zhang, H. (2019), LRRK2 and mitochondria: recent advances and current views. *Brain Res.* **1702**, 96–104. https://doi.org/10.1016/j.brainres.2018.06.010

41   Levin, R.S., Hertz, N.T., Burlingame, A.L., Shokat, K.M. and Mukherjee, S. (2016) Innate immunity kinase TAK1 phosphorylates Rab1 on a hotspot for posttranslational modifications by host and pathogen. *Proc. Natl. Acad. Sci. U.S.A.* **113**, E4776–E4783 https://doi.org/10.1073/pnas.1608355113

42   Berndsen, K., Lis, P., Yeshaw, W.M., Wawro, P.S., Nirujogi, R.S., Wightman, M. et al. (2019) PPM1H phosphatase counteracts LRRK2 signaling by selectively dephosphorylating Rab proteins. *eLife* **8**, e50416 https://doi.org/10.7554/eLife.50416

43   Waschbusch, D., Purlyte, E., Pal, P., McGrath, E., Alessi, D.R. and Khan, A.R. (2020) Structural basis for Rab8a recruitment of RILPL2 via LRRK2 phosphorylation of switch 2. *Structure* **28**, 406–417.e6. https://doi.org/10.1016/j.str.2020.01.005